

Identification of a Novel Phosphatidic Acid Binding Domain in Protein Phosphatase-1[†]

Jeffrey A. Jones,[‡] Robert Rawles, and Yusuf A. Hannun*

Molecular and Cellular Biology and Pathobiology Program and the Department of Biochemistry and Molecular Biology at the Medical University of South Carolina, Charleston, South Carolina 29425

Received March 21, 2005; Revised Manuscript Received June 29, 2005

ABSTRACT: Phosphatidic acid (PA) has been recognized as a lipid second messenger, yet few cellular targets for PA have been identified. Previous work demonstrated PA as a potent and noncompetitive tight-binding inhibitor of the catalytic subunit (γ isoform) of protein phosphatase-1 (PP1 γ) *in vitro*. The high potency of inhibition, coupled with high specificity for PA over other phospholipids, suggested the presence of a high-affinity PA binding domain on PP1 γ . In the current study, quantification of the binding interaction and identification of the binding domain were pursued. Surface plasmon resonance was employed to quantitate the interaction between PP1 γ and immobilized mixed lipid vesicles of PA/phosphatidylcholine (PC) or PC alone. The data disclosed a high-affinity interaction with a K_D measured in the low (1–40) nanomolar range, consistent with the range of K_i previously obtained from *in vitro* enzymatic assays. Next, identification of the segment of PP1 necessary for PA binding was determined using a deletion mutagenesis strategy. Binding assays revealed that PP1 γ residues between 274 and 299 were required for the interaction with the lipid. When fusions of PP1 γ fragments with green fluorescent protein (GFP) were generated, it was then determined that PP1 γ residues 286–296 were sufficient to confer PA binding to GFP, a protein that does not interact with PA. The minimal PA binding domain of PP1 γ lacked similarity to the previously described PA binding segments of Raf-1 kinase and cyclic-AMP phosphodiesterase 4A1. When these results were taken together with the known crystallographic structure of PP1, they identified a novel PA binding region on PP1 γ that contains a unique loop–strand structural fold responsible for the interaction with PA.

The discovery of diacylglycerol as a regulator of protein kinase C ushered an era of investigation focusing on potential lipids capable of functioning as second messengers. Among these are various important sphingolipids and glycerol lipids that have been implicated in the regulation of cellular signaling. One such lipid of importance is phosphatidic acid (PA).¹ Since the cloning of phosphatidylcholine-specific phospholipase D (PLD), investigators have searched for targets of its metabolic product, PA. To date, only a few cellular targets of PA have been described, and as yet, no clear lipid binding motif has emerged capable of predicting interactions with PA.

Of the PA targets described, Baillie and co-workers recently identified a calcium-dependent PA binding domain on cyclic-AMP phosphodiesterase 4A1 (PDE4A1) (1). PA-specific binding of PDE4A1 is mediated by a single bifunctional α helix in the N terminus of the protein, one face of which mediates nonpolar interactions with the membrane surface, while the other face coordinates the calcium and PA–phosphate–headgroup interactions.

Ghosh et al. also described a PA binding domain in Raf-1 kinase, and they identified a 35 amino acid fragment of Raf-1 that contains two subdomains (2, 3). One subdomain consists of a tetrapeptide of positively charged amino acids thought to mediate an initial electrostatic interaction with PA. The second subdomain consists of hydrophobic amino acids, and this domain is postulated to anchor the kinase following its initial interaction with PA-enriched membranes. Changing a lysine to an alanine within the positively charged subdomain was sufficient to block translocation of Raf-1 to the membrane fraction.

Neither of these PA binding domains has been sufficient for identifying other PA binding proteins through database searches. Hence, identification of other cellular targets of PA remains a topic of great interest. Furthermore, only as

[†] This work was supported by an award from the American Heart Association and by National Institutes of Health Grant CA-87584.

* To whom correspondence should be addressed: Department of Biochemistry and Molecular Biology, Medical University of South Carolina, 171 Ashley Avenue, Charleston, SC 29425. Telephone: (843) 792-4321. Fax: (843) 792-4322. E-mail: hannun@musc.edu.

[‡] Recipient of an American Heart Association predoctoral fellowship.

¹ Abbreviations: PP1 γ , γ isoform of the catalytic subunit of protein phosphatase-1; PA, dioleoyl-phosphatidic acid; PS, dioleoyl-phosphatidylserine; PLD, phospholipase D; PDE4A1, cyclic-AMP phosphodiesterase 4A1; GFP, green fluorescent protein; GFPns, GFP no stop codon; SLUV, sucrose-loaded large unilamellar vesicles.

additional PA binding proteins are described will the task of finding a PA binding motif be accomplished.

Protein phosphatase-1 (PP1) is a serine/threonine phosphatase expressed in all eukaryotic cells and is known to be involved in a diverse number of cellular processes, including glycogen metabolism, RNA processing, and cell cycle regulation (4–8). PP1 functions in cells as a holoenzyme comprised of a single catalytic subunit bound to a single targeting/regulatory subunit (9). There are three major isoforms of the catalytic subunit (α , β/δ , and γ) sharing greater than 90% homology at the protein level. There have been more than 50 regulatory subunits described to date, most of which share a common motif [(R/K)(V/I)XF] that mediates its interaction with the catalytic subunit (9, 10). It is generally accepted that the regulatory subunit directs the holoenzyme to macromolecular complexes in the cell where PP1 activity is required. It is unclear whether the catalytic subunit binds the regulatory subunit at the site of action or whether binding causes the holoenzyme to translocate to the site of action. In most cases, activity of the catalytic subunit is inhibited upon binding of the regulatory subunit (9). The binding of subsequent factors or post-translational modification of the regulatory subunit can relieve this inhibition.

A previous study has established PA as a potent noncompetitive inhibitor of PP1 γ *in vitro* with a K_i of approximately 1 nM (11). The potency of inhibition suggested the presence of a high-affinity PA binding domain on PP1 γ . To investigate this hypothesis, binding kinetics were established for the interaction between PA and PP1 γ by using surface plasmon resonance as a measure of interaction. Furthermore, through deletion mutagenesis of PP1 γ , these findings have defined a novel PA binding domain that is both necessary for PP1 γ interaction with PA and sufficient to confer PA binding to a protein that does not normally bind PA.

EXPERIMENTAL PROCEDURES

Materials. The γ isoform of the *Escherichia coli* recombinant human catalytic subunit of PP1 (PP1 γ) was purchased from Calbiochem (La Jolla, CA). All lipids [dioleoyl phosphatidylcholine (PC), dioleoyl phosphatidylserine (PS), and dioleoyl phosphatidic acid (PA)] were purchased from Avanti Polar Lipids, Inc. (Alabaster, AL). Anti-6 \times His mouse monoclonal antibody was purchased from Clontech Laboratories (Palo Alto, CA). Anti-PP1c (E-9) mouse monoclonal antibody was obtained from Santa Cruz Biotechnology, Inc. (Santa Cruz, CA). Goat anti-mouse peroxidase was acquired from Jackson ImmunoResearch Laboratories, Inc. (West Grove, PA). The pBAD/His-B *E. coli* expression vector was purchased from Invitrogen Corporation (Carlsbad, CA). The pEGFP vector was purchased from Clontech Laboratories (Palo Alto, CA). Restriction enzymes *Xho*I, *Kpn*I, and *Hind*III were purchased from Promega Corporation (Madison, WI). Phenylmethylsulfonylfluoride (PMSF) was purchased from Sigma Chemical Company (St. Louis, MO) as were all other reagents, unless otherwise noted.

Surface Plasmon Resonance Measurements. Biosensor measurements were carried out using a Biacore 3000 Biomolecular Analyzer (Biacore AB, Uppsala, Sweden). Binding was assayed in system buffer consisting of 50 mM Tris-HCl at pH 7.4 and 20% glycerol at 25 °C. Lipid vesicles were captured on the surface of a Pioneer L1 sensor chip







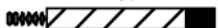
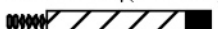
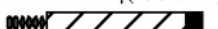
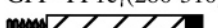
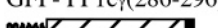
(Biacore AB, Uppsala, Sweden). The L1 sensor chip surface was first cleaned with three injections of 40 μ L of 20 mM CHAPS at a flow rate of 20 μ L/min. This was followed by two 15 μ L injections of lipid vesicles (0.2 mM total lipid concentration) at a flow rate of 2 μ L/min. Dioleoyl-PC vesicles were injected over flow cell-1 (Fc1), and a 50:50 mixture of dioleoyl-PC and dioleoyl-PA vesicles were injected over flow cell-2 (Fc2). The lipid vesicle injections reproducibly resulted in approximately 3500 RU, captured on each flow cell of the L1 surface. Purified recombinant 6 \times His-PP1 γ , diluted in system buffer, was then injected over both flow cells, using a 40 μ L Kinject command, at a flow rate of 20 μ L/min and a dissociation time of 1000 s. After each protein injection (concentrations ranging from 1.0 to 7.5 μ M), the lipid surface was stripped with two 10 μ L injections of 20 mM CHAPS at a flow rate of 20 μ L/min. New lipid surfaces were generated on each flow cell prior to the subsequent protein injection cycle. Injections were done in duplicate, and a blank injection, containing an equivalent amount of protein storage buffer diluted in system buffer, was run for each protein concentration to control for the bulk shift resulting from changes in optical density. Data were analyzed using BiaEvaluation version 3.0 software (Biacore AB, Uppsala, Sweden). The apparent association (k_a) and dissociation (k_d) rate constants were evaluated from double-referenced binding curves (Fc2–Fc1–buffer blank), assuming a 1:1 binding model ($A + B = AB$) and fit locally to account for small differences in the amount of lipid captured on the L1 surface with each new cycle. Binding constants were derived from several replicate experiments, and a representative data set is shown.

Generation of 6 \times His-Tagged PP1 γ . Human 6 \times His-PP1 γ was cloned and purified as previously described (11). The deletion and fusion mutants generated for this study are summarized in Table 1, along with the primers used for cloning each construct. Mutants were either generated by polymerase chain reaction (PCR) cloning or by PCR mutagenesis using the ExSite mutagenesis kit (Stratagene, La Jolla, CA). Primers used for PCR cloning were purchased from Integrated DNA Technologies (Skokie, IL). Primers used for ExSite mutagenesis were purchased from Qiagen-Operon (Alameda, CA). All primers were HPLC-purified, and all ExSite primers were 5'-phosphorylated.

The coding sequence for green fluorescent protein (GFP) was amplified by PCR with primers containing 5'-*Xho*I and 3'-*Kpn*I restriction sites (5' primer, CCC CTC GAG CAT GGT GAG CAA GGG CGA GGA; 3' primer, GCG GTA CCC TAC TTG TAC AGC TCG TCC ATG C), using a GFP-containing vector as a template. The product was subcloned into the pBAD/His B vector digested with the same enzymes.

PP1 γ deletion mutants [(1–176), (83–274), (165–323), and (1–299)] were constructed by PCR cloning and engineered to contain 5'-*Xho*I and 3'-*Kpn*I restriction sites. Gel-purified PCR products, generated using the indicated primer pairs, were ligated into the pCR2.1-TOPO cloning vector (Invitrogen Corporation, Carlsbad, CA). Clones containing constructs with inserts of the correct size, identified by restriction with *Xho*I and *Kpn*I, were grown and purified. The positive pCR2.1-PP1 γ mutant constructs were restriction-digested with *Xho*I and *Kpn*I, and the released inserts were gel-purified and ligated into pBAD/His B, digested with

Table 1: Proteins Generated for Use in This Study^a

Protein product/name:	PCR primer set and template used:
PP1 γ  WT	PCR primer set. Template: pGEX-6p2-PP1 γ F: CCGCTCGAGCATGGCGGATTTAGATAAACTC R: GCGGTACCCTATTTCTTTGCTTGCTTTGTG
PP1 γ (1-176)  (1-176)	PCR primer set. Template: pBAD/His-PP1 γ F: CCGCTCGAGCATGGCGGATTTAGATAAACTC R: GCGGTACCCTAACCTCCATGACAGCAGAATATCTTCTC
PP1 γ (83-274)  (83-274)	PCR primer set. Template: pBAD/His-PP1 γ F: CCGCTCGAGCCCAGAAAGCAACTACCTGTTTCTTGGGGAC R: GCGGTACCCTATCCGAATAATTGGGCGCAGAAAACAG
PP1 γ (165-323)  (165-323)	PCR primer set. Template: pBAD/His-PP1 γ F: CCGCTCGAGCGATGAGAAGATATTCTGCTGTCATGGAGGT R: GCGGTACCCTATTTCTTTGCTTGCTTTGTG
PP1 γ (1-299)  (1-299)	PCR primer set. Template: pBAD/His-PP1 γ F: CCGCTCGAGCATGGCGGATTTAGATAAACTC R: GCGGTACCCTATGCAGGCTTAAAACTGAAAAGAACAC
GFP  GFP	PCR primer set. Template: pBAD/His-PP1 γ F: CCGCTCGAGCATGGTGAGCAAGGGCGAGGA R: GCGGTACCTACTTGTACAGCTCGTCCATGC R: GCGGTACCCTTGTACAGCTCGTCCATGCCGAGAG (no stop)
GFP- PP1 γ (274-323)  GFP-(274-323)	ExSite primer set. Template: pBAD/His-GFP-PP1 γ (165-323) F: GGTACCCTTGTACAGCTCGTCCATGCCGAG R: GGAGAGTTTGACAATGCAGGTGCCATGATGAG
GFP- PP1 γ (286-323)  GFP-(286-323)	ExSite primer set. Template: pBAD/His-GFP-PP1 γ (165-323) F: GATGAAACACTAATGTGTTCTTTTCAGATTTAAAGCCTG R: GGTACCCTTGTACAGCTCGTCCATGCCGAG
GFP- PP1 γ (299-323)  GFP-(299-323)	ExSite primer set. Template: pBAD/His-GFP-PP1 γ (165-323) F: GCAGAGAAAAAGAAGCCAAATGCCACGAGAC R: GGTACCCTTGTACAGCTCGTCCATGCCGAG
GFP- PP1 γ (286-310)  GFP-(286-310)	ExSite primer set. Template: pBAD/His-GFP-PP1 γ (286-323) F: TAGAAGCTTGGCTGTTTGGCGGATGAGAG R: TACAGGTCTCGTGGCATTGCGTCTTTTCTCTG
GFP- PP1 γ (286-296)  GFP-(286-296)	ExSite primer set. Template: pBAD/His-GFP-PP1 γ (286-323) F: TAGAAGCTTGGCTGTTTGGCGGATGAGAG R: TAAAATCTGAAAAGAACACATTAGTGTTCATCCAC

^a The protein products generated and their nomenclature are indicated in the first column. The primer sets and templates used to create them are indicated in the second column. All products contain an N-terminal 6 \times histidine fusion tag. All primer sequences are shown in the 5' \rightarrow 3' orientation. F = forward primer, and R = reverse primer.

the same enzymes. Positive clones containing the final pBAD/His-PP1 γ mutant constructs were selected and verified by DNA sequencing.

Fusion mutants of GFP and PP1 γ were generated by first inserting GFPns (no stop codon) into pBAD/His B digested with 5'-*Xho*I and 3'-*Kpn*I to create pBAD/His-GFPns. PP1 γ -(165–323) was then PCR-engineered with 5'-*Kpn*I and 3'-*Hind*III restriction sites and subsequently cloned into the pBAD/His-GFPns vector, digested with the *Kpn*I and *Hind*III. The pBAD/His-GFP-PP1 γ (165–323) construct then served as a template for deletion mutagenesis using the ExSite PCR mutagenesis kit (Stratagene, La Jolla, CA), according to the protocol of the manufacturer. Positive clones were verified by DNA sequencing.

Constructs containing specific point mutations within the context of the PP1 γ (1–299) deletion and the GFP-PP1 γ -(286–296) fusion protein were generated using the ExSite PCR mutagenesis kit (Stratagene, La Jolla, CA), according to the protocol of the manufacturer. The template vectors used for site-directed mutagenesis were pBAD/His-PP1 γ -(1–299) and pBAD/His-GFP-PP1 γ (286–296). Residues Thr 288 and Ser 292 were changed to alanines, while residue

Met 290 was changed to a glutamic acid. The sequences of the primers used for site-directed mutagenesis were as follows: T288A (5' primer, GAT GAA (G)CA CTA ATG TGT TCT TTT CAG; 3' primer, CAC ACT CAT CAT GGC ACC TGC ATT GTC), S292A (5' primer, CTA ATG TGT (G)CT TTT CAG ATT TTA AAG CCT; 3' primer, TGT TTC ATC CAC AC T CAT CAT GGC ACC TGC), and M290E (5' primer, CTA (GA)G TGT TCT TTT CAG ATT TTA AAG; 3' primer, TGT TTC ATC CAC ACT CAT CAT GGC ACC). All primers used for ExSite site-directed mutagenesis were 5'-phosphorylated. The nucleic acid residues changed appear in parentheses in the 5' primers. Positive clones were verified by DNA sequencing.

The verified deletion, fusion, and point mutant constructs were used to transform TOP10 *E. coli* to allow for expression from the arabinose inducible promoter of the pBAD/His bacterial expression vector.

Expression of the 6 \times His-Tagged PP1 γ . TOP10 *E. coli* containing constructs for wild-type or mutant PP1 γ were grown to stationary phase in overnight cultures. They were then diluted and allowed to grow for 2 h to reach log-phase growth. The bacterial cells were then induced with the

addition of L-arabinose (concentrations ranging from 0.0002 to 0.2% in Lauria–Bertani medium containing 60 $\mu\text{g/mL}$ ampicillin) and allowed to grow for 4 h before 2 mL of each culture was harvested by centrifugation. Uninduced lysates (PP1 γ and GFP) were also processed and used to control for nonspecific interactions. The bacterial cell pellets were resuspended in lysis buffer containing 50 mM Tris-HCl at pH 7.4, 100 μM MnCl₂, and 20% glycerol. The cells were lysed by 5 cycles of freeze (dry-ice methanol bath)/thaw (42 °C water bath), followed by sonication with a probe-tip sonicator (1 \times 60 s at 8% power). The bacterial lysates were centrifuged at 100000g for 1 h at 4 °C, and 0.1 mM PMSF was added to the recovered supernatants. High-speed lysates were stored at –70 °C until used.

Preparation of Sucrose-Loaded Large Unilamellar Vesicles (SLUV). Lipid vesicles were generated on the basis of a previously published method (12). Briefly, lipids were dried in glass tubes from chloroform stocks (10 mg/mL) under a stream of nitrogen gas. The dried lipids were then placed in a vacuum desiccator for 30 min at room temperature to remove all traces of organic solvent. The dried lipids were then hydrated in 10 mM Tris-HCl at pH 7.4, 20 mM KCl, and 180 mM sucrose for 30 min at room temperature. The hydrated lipids were vortexed for 2 min continuously and then subjected to 5 freeze (dry-ice methanol bath)/thaw (42 °C water bath) cycles. The resulting sucrose-loaded vesicles were then extruded through polycarbonate filters with a 0.1 μm pore diameter (100 mol % vesicles) or a 0.4 μm pore diameter (PC/PA mixed vesicles). The lipid vesicles were extruded 21 times, using the Avanti mini-extruder (Avanti Polar Lipids, Alabaster, AL) to generate unilamellar vesicles of uniform size. The resulting SLUV were subjected to centrifugation at 100000g for 1 h at 4 °C. The pellet was resuspended in SLUV binding buffer (50 mM Tris-HCl at pH 7.4 and 150 mM KCl) to a concentration of 1 mM total lipid and stored at 4 °C until used. Lipids were prepared and used on the same day.

SLUV Binding Assay. Binding assays were performed using a modified protocol of a previously published method (12). The standard binding assay contained 0.5 mM lipid delivered in vesicle form, in 50 mM Tris-HCl at pH 7.4 with 150 mM KCl. Purified commercially available PP1 γ (Calbiochem, San Diego, CA) or soluble bacterial lysate expressing wild-type 6 \times His-PP1 γ or a 6 \times His-tagged mutant of PP1 γ was added to each reaction tube. To normalize each reaction for the amount of expressed 6 \times His-tagged protein, 3 μg of total protein from the high-speed bacterial lysate of 6 \times His-PP1 γ was used per binding reaction and the input protein for all other binding reactions was normalized to the wild type by comparing the amount of expressed protein by Western blotting with anti-6 \times His antibody. 6 \times His-tagged GFP was used as a control for nonspecific protein binding. The binding reactions were incubated for 20 min at 30 °C. They were then immediately transferred to a cold (4 °C) TLA45 rotor and centrifuged in a Beckman tabletop ultracentrifuge at 100000g for 1 h. The resulting supernatant (representing the nonbound fraction of protein) and the lipid pellet (representing the bound fraction of protein) were collected separately and analyzed by SDS–PAGE. The protein fractions were transferred to PVDF membranes (Bio-Rad Laboratories, Hercules, CA) and identified by immunostaining with anti-PP1c or anti-6 \times His

monoclonal antibody. The protein bands were visualized by ECL (Amersham Biosciences Corporation, Piscataway, NJ) and recorded on XOMAT MR film (Eastman Kodak Company, Rochester, NY).

Database Searches. The amino acid sequence for PP1 γ (286–323) was used in a BLAST search against the Protein Information Resource and SwissProt databases using the SeqWeb version 2.1 web-based sequence analysis interface for the Genetic Computer Group (GCG) Wisconsin Package version 10.3 analysis software (Accelrys, Inc., San Diego, CA). Similarly, GCG was also used to perform sequence alignments with the PA binding domains from Raf-1 and PDE4A1. Structural data of PP1 γ were obtained from the Protein Data Bank (PDB 1jk7). The sequence comparison with secondary structure was obtained from the PDBSum web site (<http://www.biochem.ucl.ac.uk/bsm/pdbsum/>). The secondary structure for PP1 γ (224–323) and Raf1-C (390–426) was predicted using The PredictProtein Server (<http://cubic.bioc.columbia.edu/predictprotein>) and PHDsec analysis (13–15). For structural domain searching, PDB coordinates were extracted from PDB 1jk7 using the MaxSprout web-based tool (<http://www.ebi.ac.uk/maxsprout/>). Coordinates for PP1 γ (269–299) were then submitted to the DALI server (<http://www2.ebi.ac.uk/dali/>) to identify other proteins of known structure that may contain similar secondary structure to the identified PA binding domain.

Generation of PP1 γ Structures. The crystal structure of PP1 γ complexed with okadaic acid (solved by Maynes et al. (16); PDB 1jk7) was used to generate three-dimensional images and molecular surfaces for structural analysis using the software package Sybyl version 6.9 (Tripos, Inc., St. Louis, MO). The Connolly molecular surface was mapped for lipophilic potential and colored accordingly (with brown indicating areas of increased hydrophobicity and blue indicating areas of increased hydrophilicity). All water molecules and heteroatoms were removed from the structure prior to generating the molecular surface.

RESULTS

Analysis of PP1 γ Binding to Immobilized PA Vesicles by Surface Plasmon Resonance. Previously, it was demonstrated that PA is a potent and highly specific inhibitor of PP1 γ (11). Furthermore, the kinetics of inhibition were consistent with a tight-binding noncompetitive mechanism. In an effort to further characterize this interaction, binding studies were performed by measuring surface plasmon resonance on a Biacore 3000 biosensor.

Initial attempts were made to quantitate the interaction between PA and PP1 γ by immobilizing 6 \times His-PP1 γ on the surface of a CM5 sensor chip coated with anti-pentaHis antibody. Although the injection of PA vesicles displayed dose-dependent binding to the immobilized protein, difficulties in obtaining a stable baseline of protein bound to the antibody made the quantitation of the data unreliable (data not shown). As an alternative, the Pioneer L1 chip allowed for the stable immobilization of lipid vesicles, over which was passed purified recombinant human 6 \times His-PP1 γ . Several concentrations of protein, ranging from 1.0 to 7.5 μM , were assayed for binding by passing them over a control surface of PC vesicles immobilized on Fc1 and over a sample surface of mixed PA/PC (50:50) vesicles immobilized on

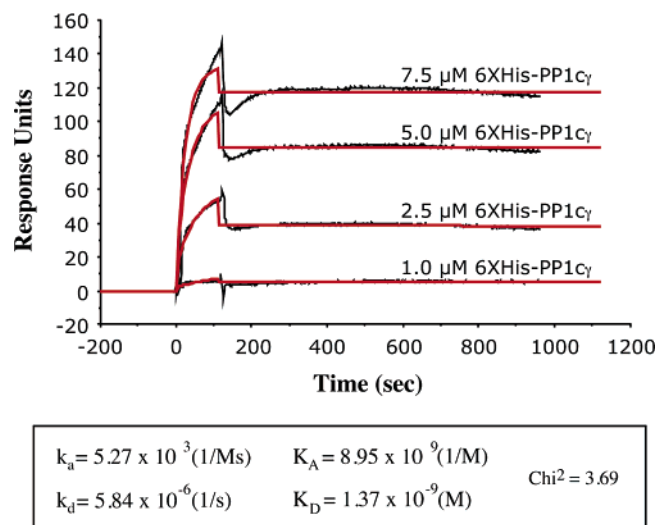


FIGURE 1: Quantitative binding analysis of the interaction between PP1 γ and PA. Lipid vesicles were immobilized on a Pioneer L1 sensor chip. PC (100 mol %) vesicles were loaded on Fc1, and PC/PA (50:50 mol %) vesicles were loaded on Fc2. Various concentrations of purified recombinant PP1 γ were injected over the surface at 20 μ L/min. The plot shows the differential binding (Fc2–Fc1–buffer blank) of PP1 γ to PA in black. For kinetic analysis, the differential binding curves were approximated by nonlinear regression using BIAevaluation software (fit curves shown in red). The calculated kinetic values are shown below the plot along with the χ^2 value for the comparison of the fit versus actual binding curves. Data shown are the best-fit data set from several replicate experiments.

Fc2. Fc1 was used to control for nonspecific protein–lipid interactions, and a buffer blank was additionally subtracted from the sensorgram to control for nonspecific changes in the refractive index. Upon injection of the recombinant protein, no binding of 6 \times His-PP1 γ was observed in Fc1. On Fc2, however, 6 \times His-PP1 γ bound dose-dependently to PA/PC vesicles and displayed very slow dissociation (Figure 1).

Binding kinetics were calculated using the BIAevaluation software version 3.0. The binding of 6 \times His-PP1 γ displayed an association rate range of 5.27×10^3 to $1.32 \times 10^3 \text{ Ms}^{-1}$, a dissociation rate range of 5.84×10^{-6} to $8.81 \times 10^{-6} \text{ s}^{-1}$, and an equilibrium association constant range of 8.95×10^9 to $8.15 \times 10^8 \text{ M}^{-1}$. The slow dissociation of 6 \times His-PP1 γ from the PA/PC surface is consistent with a tight-binding model and yielded an overall K_D range of 1.37×10^{-9} to $38.47 \times 10^{-9} \text{ M}$. These data support the hypothesis that PP1 γ must contain a high-affinity lipid-binding domain for PA.

Identification of a PP1 γ Segment Necessary for PA Binding. Because many previously described lipid-binding domains have been comprised of a discrete series of amino acids (C2 domain, PS binding domain of ISC1p, FYVE, and others), the task of identifying the PA binding domain in PP1 γ was approached with the assumption that a defined segment of amino acids could mediate the interaction between the lipid and protein. To identify regions of PP1 γ capable of mediating the interaction with PA, a binding assay was employed using SLUV incubated with bacterial lysates expressing wild-type or mutant 6 \times His-PP1 γ or purified commercially available PP1 γ . After a predetermined time of interaction, the vesicles were isolated by centrifugation at 100000g. Protein bound to the vesicles was found

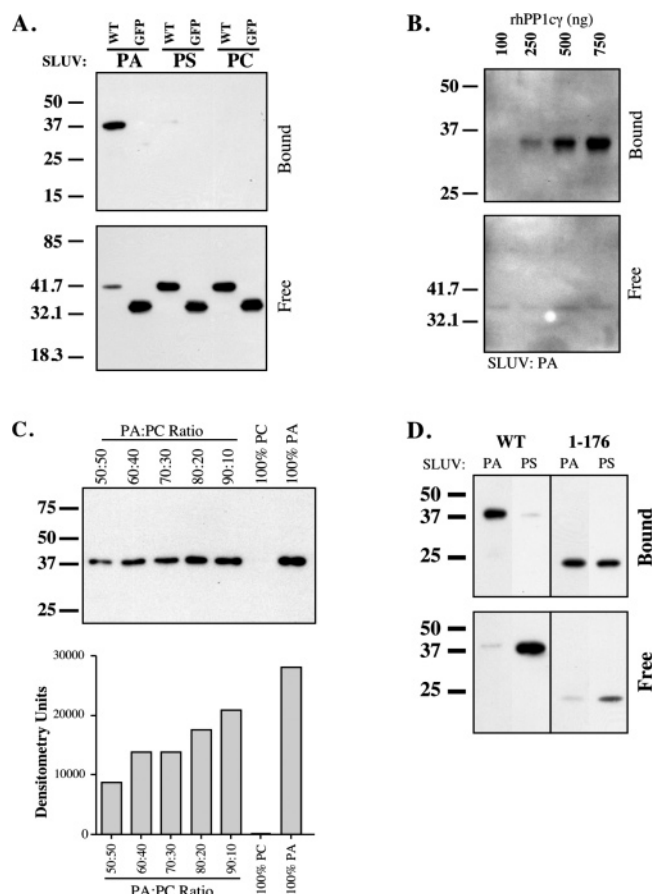


FIGURE 2: Specificity of PP1 γ binding to PA. SLUV binding assays were performed to assess specificity of PP1 γ binding to vesicles of PA. (A) 6 \times His-PP1 γ (WT) and 6 \times His-GFP (GFP) interaction with PA, PS, or PC vesicles. (B) Dose-dependent binding of commercially available nontagged recombinant PP1 γ with PA–SLUV. (C) (Top) Dose-dependent binding of 6 \times His-PP1 γ to varying amounts of PA incorporated in mixed PA/PC vesicles and (bottom) densitometry of 6 \times His-PP1 γ binding to mixed PA/PC vesicles. (D) Comparison of 6 \times His-PP1 γ and 6 \times His-PP1 γ (1–176) binding to PA– and PS–SLUV. The results shown are representative of at least two replicate experiments.

associated with the lipid pellet, whereas nonbinding proteins remained in the supernatant.

To verify the functionality of the SLUV binding assay using bacterial lysates as the source of recombinant protein, binding between PA and PP1 γ was first evaluated for specificity. As can be seen in Figure 2A, a lysate expressing wild-type full-length 6 \times His-PP1 γ (WT) displayed significant binding to SLUV made with dioleoyl-PA (PA–SLUV); 6 \times His-tagged protein was associated with the lipid pellet following centrifugation, while little remained in the supernatant.

To verify that the specific binding was not due to PA interactions with the histidine tag, a lysate expressing 6 \times His-GFP (GFP) was also assayed for binding. Figure 2A shows that all of the 6 \times His-GFP protein was observed in the supernatant following centrifugation, providing evidence that the interaction between 6 \times His-PP1 γ and PA–SLUV is not simply mediated by the histidine tag and suggesting that there is a specific interaction between PP1 γ and PA that cannot be duplicated by another globular protein. Furthermore, to demonstrate that the interaction between PA and PP1 γ shows specificity for PA over other lipids, lysates expressing

WT or GFP were likewise incubated with SLUV made from either dioleoyl-PS (PS-SLUV) or dioleoyl-PC (PC-SLUV). The data in Figure 2A also reveal that neither of the expressed proteins was able to bind to PS-SLUV or PC-SLUV, indicating that the interaction between 6 \times His-PP1 γ and PA-SLUV is specific for PA, which also agrees with previously published lipid-protein overlay data (11). Moreover, because the SLUV preparations were extruded through polycarbonate filters and purified by centrifugation, differences in the vesicle size and density were minimized, lending confidence that the binding specificity achieved was not influenced by a noncontrollable biophysical property of the phospholipids but by the selectivity of the interacting region within PP1 γ . Additionally, when PA-SLUV was incubated with non-histidine-tagged commercially available recombinant human PP1 γ , dose-dependent binding of the protein was observed (Figure 2B), again confirming that there is a direct interaction between PP1 γ and PA and that this interaction is independent of the histidine tag or of any contaminating bacterial protein.

In an effort to determine the optimal concentration of PA required for high specificity binding, 6 \times His-PP1 γ binding was assessed to lipid vesicles containing a varying mole percentage of PA in mixed PA/PC SLUV. The data in Figure 2C revealed that 6 \times His-PP1 γ bound dose-dependently, such that as the PA concentration in the mixed PA/PC vesicles increased so did the amount of bound 6 \times His-PP1 γ . Moreover, SLUV made with 100% PA was found to bind the greatest amount of 6 \times His-PP1 γ . Because this assay relies on the nonquantitative assessment of binding to identify regions of lipid interaction within the protein, maximizing the binding of 6 \times His-PP1 γ to PA-SLUV was highly desired. Hence, to achieve the highest lipid binding specificity, all subsequent binding reactions were assessed using SLUV comprised of 100% PA.

To localize the PA-specific binding domain in PP1 γ , a series of 6 \times His-tagged PP1 γ deletion mutants were generated and used in SLUV binding assays. It was of concern, however, that, upon gross deletion of large portions of the protein, many hydrophobic domains buried during protein folding may become exposed to the surface and mediate nonspecific interactions with the sucrose-loaded vesicles. In an attempt to circumvent misinterpretation of binding results, we performed SLUV binding assays in the presence of a second anionic phospholipid, PS-SLUV, to determine nonspecific hydrophobic interactions. As can be seen in Figure 2C, 6 \times His-PP1 γ (1–176) binds to both PA-SLUV and PS-SLUV. From a previous study, PS was unable to inhibit PP1 γ activity and displayed no interaction with 6 \times His-PP1 γ in a protein-lipid overlay assay (11). Furthermore, results from Figure 2A also show that the full-length His-tagged enzyme does not bind PS-SLUV. Hence, by including the PS-SLUV results, binding data is controlled for both non-PA-specific binding because of general hydrophobic interactions as well as interactions with other anionic phospholipids that do not occur with the full-length enzyme. Thus, any protein construct binding to PS vesicles was considered uninformative toward defining the PA-specific binding domain, as demonstrated by the protein fragment 6 \times His-PP1 γ (1–176).

With these considerations in mind, the SLUV binding results for the initial set of deletion mutants are shown in

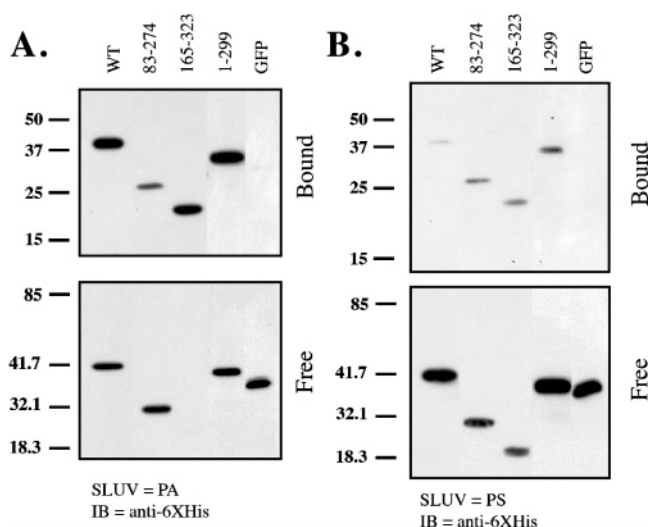


FIGURE 3: SLUV binding assays with 6 \times His-PP1 γ deletion mutants. SLUV binding assays were performed to assess binding of 6 \times His-GFP (GFP), 6 \times His-PP1 γ wild type (WT) and various 6 \times His-PP1 γ deletion mutants to (A) PA-SLUV or (B) PS-SLUV. Representative results shown from at least three replicate experiments.

Figure 3. Bacterial lysates expressing WT, GFP, or the 6 \times His-PP1 γ mutants, 83–274 and 165–323, were assayed for binding to both PA and PS vesicles.

Figure 3A shows that WT and 6 \times His-PP1 γ (165–323) displayed significant binding to PA-SLUV, while the 83–274 fragment and GFP displayed little interaction. When the same constructs were assayed for PS-SLUV binding, no significant interaction was observed for any of the constructs. Together, these data suggest that the PA-specific binding domain resides in the 165–323 fragment.

To further narrow the segment of PP1 γ necessary for PA binding, C-terminal deletions of PP1 γ were generated and assayed for PA- and PS-SLUV binding. Figure 3A, further reveals that 6 \times His-PP1 γ (1–299) binds PA-SLUV, while Figure 3B demonstrates specificity for PA, because little PS-SLUV binding was observed. Further deletion at the C terminus yielded uninterpretable results because PA-specific binding was lost and significant interactions with both PA- and PS-SLUV were observed for the 6 \times His-tagged deletion fragments of PP1 γ (1–274, 1–279, 1–286, and 1–290) (data not shown). Thus, destabilizing the C terminus through large deletions may result in an unstructured domain that binds nonspecifically to hydrophobic molecules.

Overall, these results suggest that the C terminus of PP1 γ harbors a domain capable of mediating its interaction with PA vesicles and that the segment between amino acid residues 274 and 299 appears to be necessary to achieve specific PA binding.

Identification of PP1 γ Segments Sufficient for PA Binding. Next, in an effort to define segments of PP1 γ sufficient for interacting specifically with PA, small segments of PP1 γ were fused to 6 \times His-GFP to identify fragments capable of conferring PA-specific binding to this protein that has previously been shown not to interact with PA- or PS-SLUV (Figure 2A). From the deletion study, we identified that the C terminus of PP1 γ was necessary for PA binding; hence, the initial segments tested were chosen from assessing the three-dimensional crystal structure and choosing segments that were found to lie on the surface of the protein, where

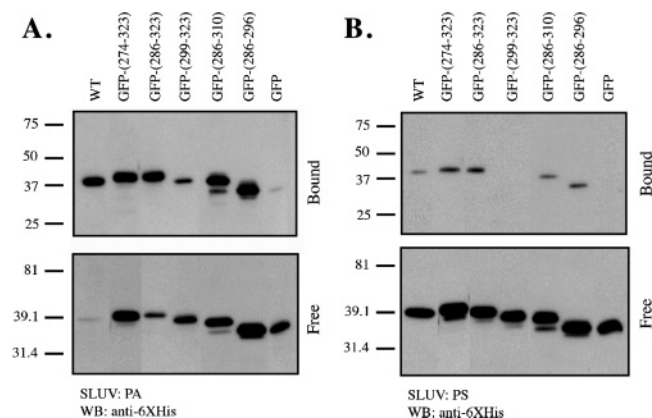


FIGURE 4: SLUV binding assays with 6 \times His-GFP-PP1 γ mutant fusions. SLUV binding assays were performed to assess binding of 6 \times His-GFP (GFP), 6 \times His-PP1 γ wild type (WT), and fusions of PP1 γ fragments to the C terminus of 6 \times His-GFP. (A) PA-SLUV or (B) PS-SLUV. Representative results shown from at least two replicate experiments.

they were capable of mediating interactions with lipid vesicles. To this end, fusions of 6 \times His-GFP-PP1 γ (274–323) and (286–323) displayed robust binding to PA-SLUV, whereas 6 \times His-GFP-PP1 γ (299–323) showed a severely diminished interaction (Figure 4A).

Moreover, none of these fragments displayed significant PS-SLUV binding (Figure 4B). From these results, it can be concluded that the segment of PP1 γ between residues 286 and 323 is sufficient to impart specific PA binding to 6 \times His-GFP.

To identify a minimal domain capable of interacting with PA, additional GFP fusions were generated from C-terminal deletions of the PP1 γ (286–323) fragment. PA- and PS-SLUV binding assays were completed with 6 \times His-GFP-PP1 γ (286–310) and (286–296) (parts A and B of Figure 4). The data demonstrate that both fragments bind PA-SLUV and show no specificity for PS-SLUV, suggesting that a fragment as small as PP1 γ (286–296) is capable of conferring PA-specific binding to GFP. Interestingly, the amount of protein bound to PA, relative to the soluble unbound protein, diminished as the domain was shortened; more unbound protein was observed in the free fraction as the putative domain decreased in size from 286–323 to 286–310 to 286–296 (Figure 4A). These data indicate that the GFP-PP1 γ (286–296) fragment has approached a minimal binding domain that is both necessary and sufficient to bind PA vesicles.

Identification of Critical Residues in PP1 γ Involved in PA Binding. To identify critical residues involved in PA binding within the localized minimal PA binding region of PP1 γ , point mutations were generated by site-directed mutagenesis. It was previously determined from *in vitro* activity assays that the catalytic subunit of PP2A (PP2Ac) was only minimally inhibited by PA (unpublished observations). Because PP1 γ and PP2Ac retain approximately 44% amino acid sequence identity, upon amino acid sequence alignment, common residues falling within the aligned minimal PA binding domain of PP1 γ were identified as potential critical residues in full-length PP1 γ for mediating high-affinity interactions with PA (Figure 5A).

Because the PP1 γ (1–299) deletion retained phosphatase activity, was still inhibitable by PA (data not shown), had a

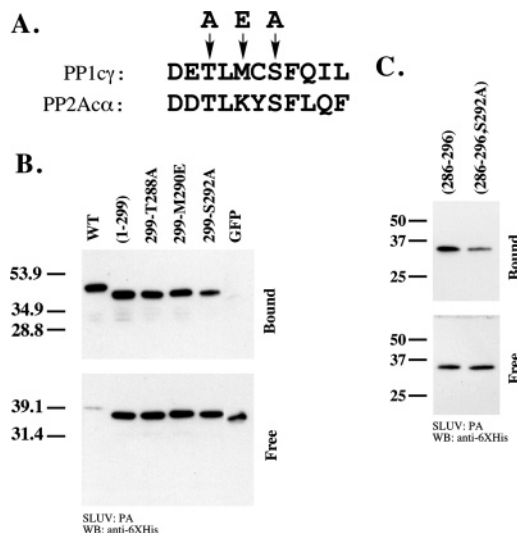


FIGURE 5: SLUV binding assays of point mutants in the minimal PA binding domain. (A) Identification of potentially important amino acid residues found in the minimal PA binding site identified in PP1 γ from the amino acid sequence alignment of PP1 γ and PP2Ac α . (B) PA-SLUV binding results for 6 \times His-PP1 γ (WT), 6 \times His-PP1 γ (1–299) (1–299), 6 \times His-PP1 γ (1–299, T288A) (299-T288A), 6 \times His-PP1 γ (1–299, M290E) (299-M290E), and 6 \times His-PP1 γ (1–299, S292A) (299-S292A). (C) PA-SLUV binding results for GFP-PP1 γ (286–296) (286–296) and GFP-PP1 γ (286–296, S292A) (286–296, S292A). Representative results shown from at least two replicate experiments.

known structure based on crystallographic studies, and preserved specific PA-SLUV binding, the point mutations were generated in this construct to simplify analysis. Hence, threonine 288 and serine 292 were changed to alanine residues (T288A and S292A), while methionine 290 was changed to a glutamic acid residue (M290E). Binding assays were performed with both PA-SLUV and PS-SLUV, and as observed in Figure 5B, the data demonstrate that, while the T288A and M290E point mutation have little effect on PA-SLUV binding of the PP1 γ (1–299) fragment, the PP1 γ (1–299, S292A) point mutant significantly reduced the amount of interaction with PA-SLUV. No appreciable PS-SLUV binding was observed for any of the constructs (data not shown). To verify the importance of the serine in the PP1 γ (286–296) minimal PA binding region, the S292A mutation was subsequently generated in the GFP-PP1 γ -(286–296) fusion construct. Figure 5D demonstrates that PA-SLUV binding is severely diminished upon introducing the S292A mutation.

When these data are taken together, they confirm that PP1 γ (286–296) is a bona fide PA binding region localized in the C terminus of PP1 γ and that upon mutating serine 292 to alanine, binding to PA can be modulated.

DISCUSSION

Previous data have identified PP1 γ as a potential target of PA *in vitro*, demonstrating potent inhibition of enzyme activity, with the highest K_a thus far described for an *in vitro* target for PA. In this study, high-affinity binding of PP1 γ to PA has been demonstrated and a PA binding domain was identified that is both necessary and sufficient to mediate the interaction between the protein and lipid. These data are important because (1) they corroborate and extend previous results suggesting a high-affinity interaction between PP1 γ

and PA and (2) they define a novel PA binding region that may contribute toward the identification of a consensus PA binding motif.

The task of studying lipid–protein interactions is often fraught with difficulties stemming from the hydrophobicity of the interacting molecules. Employing specialized techniques, one can begin to assess binding interactions; however, vigilance is required to distinguish specific and nonspecific interactions. To compensate for this difficulty, a number of complementary approaches may be required because each of the procedures/assays has its own limitations. In this study, a biomolecular sensor was employed to detect and quantify the binding interaction between PP1 γ and PA. On the other hand, the use of SLUV allowed for rapid detection and qualitative assessment of binding. These complemented and extended our previous results utilizing enzymologic assessment of the interaction and lipid–protein overlay assays (11).

In the previous study, by overlay assay, it was demonstrated that PP1 γ bound PA with high specificity for the lipid; however, limitations imposed by immunodetection of protein binding prevented accurate quantitation of kinetic binding parameters. Similarly, the enzymologic assessment of PP1 γ inhibition by PA allowed for the quantitative description of the inhibition of activity and disclosed a high-affinity tight-binding mechanism but did not directly measure the physical interaction between the protein and lipid. Therefore, the first goal of this study was the task of quantitating PA–PP1 γ binding using a Biacore 3000 biosensor and surface plasmon resonance, as a highly sensitive method for the measurement of binding interactions in real time.

The Pioneer L1 sensor chip was employed to measure 6 \times His–PP1 γ binding to immobilized lipid vesicles. Quantitative data was obtained with intensive optimization of the conditions by altering the system buffer, the composition of the immobilized vesicles, and the chip regeneration conditions. Ultimately, it was demonstrated that PP1 γ binds to an immobilized PA/PC surface in a dose-dependent fashion, whereas no binding was observed to PC alone. Interestingly, high concentrations of protein were required to overcome an initial slow association rate; however, once bound, protein dissociation from the lipid surface was very slow. Importantly, data from the plasmon resonance studies demonstrating an equilibrium dissociation constant falling within the range of 1–40 nM is very consistent with our enzymologic results that showed a K_i for PA of approximately 1 nM.

Quantitative demonstration of a high-affinity interaction supported the hypothesis that a high-affinity PA binding domain was present on PP1 γ . Hence, the second goal of this study was to locate and identify this high-affinity PA binding domain. A summary of the PA-specific binding data is shown in Figure 6.

The initial deletion study suggested that the region between residues 274 and 299 was necessary for PA-specific binding. To further investigate the importance of that region, smaller segments of PP1 γ were fused to 6 \times His–GFP to identify a minimal segment capable of conferring PA binding to this non-PA-interacting protein. Ultimately the binding data demonstrated that 6 \times His–GFP–PP1 γ (286–296) could bind PA with high specificity. Furthermore, it was observed that, as the fusion segment was shortened, less overall PA binding was observed, suggesting that a minimal PA binding domain







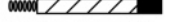



Name	Protein Product	PA-specific Binding
WT		+++
(83-274)		–
(165-323)		+++
(1-299)		+++
GFP		–
GFP-(274-323)		++
GFP-(286-323)		+++
GFP-(299-323)		+
GFP-(286-310)		++
GFP-(286-296)		++

FIGURE 6: Summary of SLUV binding data. Summary of PA-specific SLUV binding data. +++, ++, and + indicate a qualitative assessment of PA-specific binding in decreasing intensity, and – indicates that binding was not specific for PA. Gray ellipses represent the 6 \times histidine tag. Black bars represent PP1 γ or the PP1 γ deletion fragments. Hatched bars represent full-length GFP.

was being approached. This minimal domain was found to be both necessary and sufficient to mediate the interaction between PP1 γ and lipid vesicles of PA.

Most importantly, upon generation of a point mutant (S292A) within the minimal binding region, PA binding was diminished, identifying Ser 292 as a critical residue involved in mediating this specific interaction with PA.

Figure 7 shows several representations of the structure of human PP1 γ . The data are based on crystallographic analysis performed by Maynes and co-workers who crystallized human PP1 γ in the presence of okadaic acid (16). It should be noted that, although full-length PP1 γ was crystallized, residues 1–5 and 300–323 failed to be localized in the electron-density map. A comparison of the amino acid sequence to the secondary structure is shown in Figure 7A.

The identified PA binding region was comprised of an 11 amino acid segment of PP1 γ , containing mainly nucleophilic and hydrophobic amino acids. This was somewhat surprising based on the previously published PA binding domain identified in the Raf1 kinase (2). Interactions between Raf1 and PA are mediated by a short tetrapeptide of positively charged residues followed by a short stretch of hydrophobic residues. The lack of basic residues within the minimal PA binding domain of PP1 γ was unexpected; however, the proximity of a poly-basic region in residues 297–303, as well as many of the basic residues found between amino acids 304 and 323, may likely contribute to the overall PA binding domain (Figure 7A). This implication was supported by data showing the diminished yet specific PA binding of the 6 \times His–GFP–PP1 γ (299–323) fusion fragment (Figure 4). Thus, the physical characteristics of the PA binding domain on PP1 γ somewhat reflect the domain described for Raf-1 kinase. The lack of structural data for the PP1 γ residues 300–323 prevent direct conclusions of the localization of the C terminus; however, the presence of five proline residues in this region suggests that the C-terminal tail could fold back alongside the minimal binding domain to form a more complete PA binding site. This hypothesis is supported by a secondary structure prediction showing that residues 300–323 lack helical or β -strand structure (PHDsec Analysis, Figure 7A). Therefore, the full PA binding domain on PP1 γ likely consists of the residues comprising the minimal domain (286–296) as well as

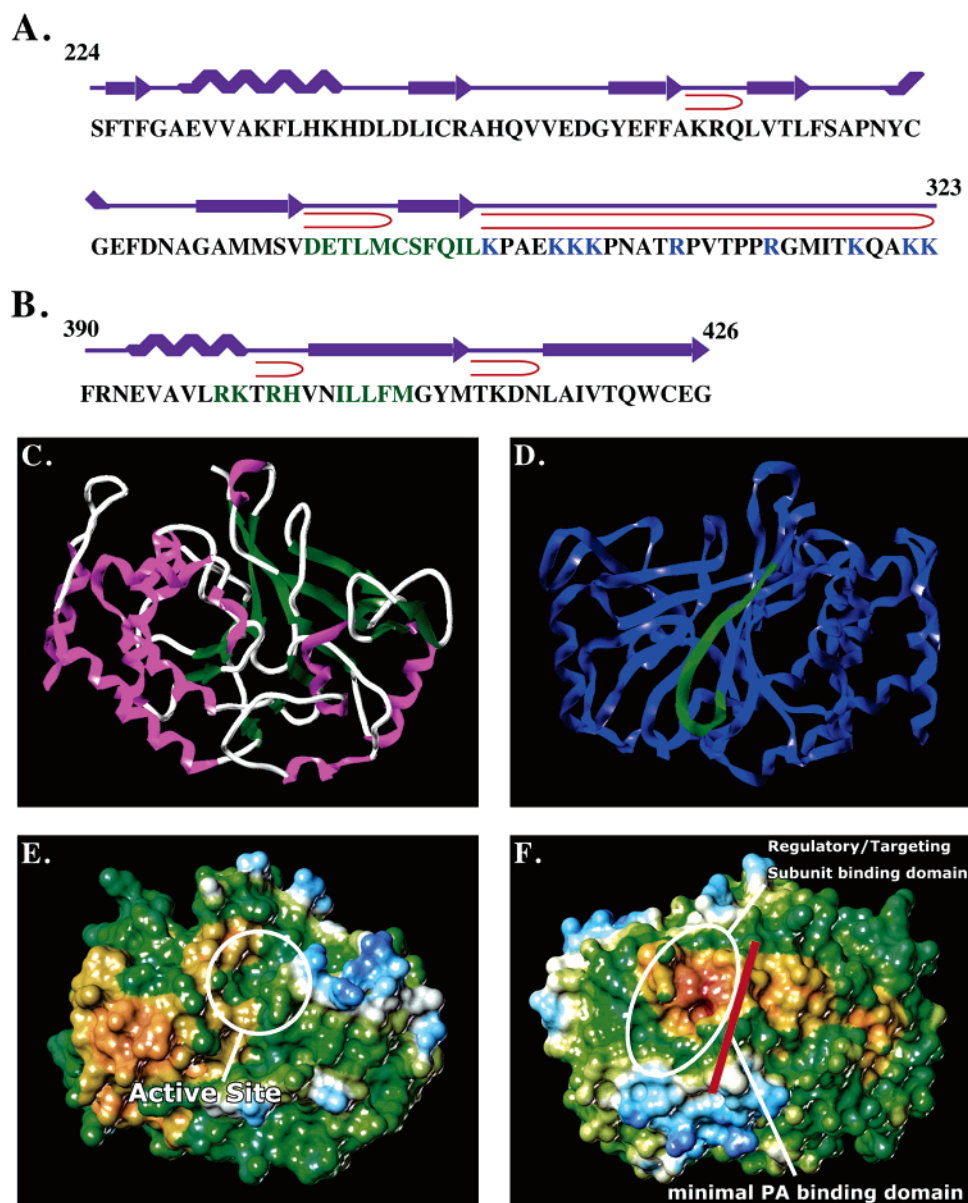


FIGURE 7: Structure and localization of the PA binding domain on PP1 γ . The structure of human PP1 γ crystallized in the presence of okadaic acid (Maynes et al.; PDB 1jk7) was used for structural localization of the PA binding domain. (A) Sequence of the C terminus of PP1 γ (residues 224–323). The sequence is overlaid with representations of the known secondary structure (224–299) and predicted secondary structure (300–323). The minimal PA binding domain is highlighted in green, and basic residues of the C terminus are highlighted in blue. (B) Sequence of the C-terminal residues 390–426 of Raf1-C overlaid with a representation of the predicted secondary structure. The core residues of the PA binding domain are shown in green. (C) Ribbon diagram showing the substrate binding domain and active site. (D) Ribbon diagram showing the targeting/regulatory subunit binding site and the minimal PA binding domain colored in green. Representation is on the opposite side of the enzyme from the active site. (E) Connolly molecular surface colored according to lipophilic potential (brown indicates increased hydrophobicity, and blue indicates increased hydrophilicity). Same representation as shown in C. The active site is highlighted. (F) Connolly molecular surface colored according to lipophilic potential. Same representation as depicted in B. The targeting/regulatory subunit binding site and the PA binding domain are highlighted.

residues present in the C-terminal tail of PP1 γ , which together present a more complicated tertiary binding structure (Figure 7A). Hence, the minimal PA-specific binding region identified in this study, while both necessary and sufficient for mediating specific interactions with vesicles of PA, is most likely a subset of the complete PA binding domain. Elucidation of the complete domain will likely be difficult using a point-mutation strategy if its structure is determined by a tertiary sequence of amino acids. Therefore, further analysis will focus on cocrystallizing PA with the full-length enzyme in an effort to circumvent these difficulties.

Ribbon diagrams of PP1 γ depicting the face of the enzyme including the substrate binding domain and the active site are shown in Figure 7C, whereas the opposite side of the enzyme that includes the targeting/regulatory subunit-binding site is shown in Figure 7D. The previous study establishing PA as a noncompetitive inhibitor of PP1 γ is supported by the localization of the minimal PA binding domain at a site distinct from the active site; residues 286–296 are located on the face of the enzyme opposite from the active site (Figure 7D). Analysis of the secondary structure of residues 286–296 revealed that the minimal PA binding

domain is comprised of a loop-strand fold that may constitute a novel structural motif required for PA binding (parts A and D of Figure 7).

Attempts to identify other PA binding proteins using the PP1 γ -minimal PA binding domain failed to return significant hits when amino acids 286–323 were blasted against a protein database. Furthermore, to ascertain whether the loop-strand fold is common among other proteins of known structure, PDB coordinates for residues 269–299 were submitted to the DALI server for structural comparison. No proteins in the database, other than PP1 γ , were identified that contained this structural fold (see the Experimental Procedures for details), suggesting that the PA binding domain of PP1 γ may be novel in sequence and structure.

Although no crystal structure is available for the full-length Raf-1 protein nor for the domain containing its PA binding site, structural prediction of the Raf-1 minimal PA binding domain (PHDsec analysis and ref 2) reveals that the positively charged residues lie at the end of a helix and within a small loop structure, whereas the hydrophobic residues lie at the beginning of a β strand (Figure 7B). Thus, the structure of the PA binding domain of Raf-1 may share some common structural features with the PA binding domain of PP1 γ , displaying a similar loop-strand fold. In contrast, the PA binding domain of PDE4A1 is found on a bifunctional helical domain and bears no resemblance to the PA binding domains of PP1 γ or Raf-1 by physical characteristics, sequence, or structure (1). It should be noted as well that PDE4A1 requires both a pair of tryptophan residues for membrane anchoring and calcium for interaction with PA, representing a unique PA binding mechanism that bears closer resemblance to a C2 domain. Hence, the identification of this non-calcium-requiring novel loop-strand fold may indicate that proteins that interact directly with PA contain a common structural motif.

Connolly surface projections of the ribbon diagrams displayed in parts C and D of Figure 7 were generated and colored according to lipophilic potential (parts E and F of Figure 7, respectively). The brown patches indicate areas of higher hydrophobic potential, whereas the blue areas are more hydrophilic. Figure 7F shows an area of increased hydrophobicity at the site of interaction between the catalytic subunit and the targeting/regulatory subunits. Interestingly, the minimal PA binding domain identified in this study maps to a ridge defining one edge of the regulatory subunit binding site. This is intriguing given that most of the regulatory subunits binding at this location also inhibit enzyme activity. This likewise suggests that PA may function as a “pseudo-targeting subunit”, docking and inhibiting the enzyme at membrane surfaces enriched in PA. Moreover, Ito and co-workers previously demonstrated that the myosin binding regulatory subunit of PP1 was capable of binding PA (17). It is thus intriguing to hypothesize that the complete PA binding domain may be comprised of an intermolecular tertiary site formed by a partial domain present in the catalytic subunit and a partial domain present in a regulatory subunit, as has recently been described for an intermolecular PH-like domain generated by the interaction of phospholipase C and its binding partner TRPC3 (18).

In this paper, the presence of a novel high-affinity PA binding domain on the surface of PP1 γ has been confirmed through kinetic binding analysis. Furthermore, through the

use of high specificity sucrose-loaded vesicle binding assays, analysis of deletion and fusion fragments of PP1 γ led to the identification of a minimal PA-specific binding region localized to PP1 γ (286–296). Disruption of the minimal PA binding region by introduction a single-point mutation was found to be sufficient to dramatically reduce PA binding. Additional studies will be required to identify and elucidate the complete high-affinity PA binding domain within PP1 γ and to establish its impact on phosphatase regulation in cells.

ACKNOWLEDGMENT

The authors wish to thank the Medical University of South Carolina Biomolecular Resource Facility (W. Scott Argraves, director) and Christian Knaak for helpful discussions and assistance with Biacore experimentation.

REFERENCES

- Baillie, G. S., Huston, E., Scotland, G., Hodgkin, M., Gall, I., Peden, A. H., MacKenzie, C., Houslay, E. S., Currie, R., Pettitt, T. R., Walmsley, A. R., Wakelam, M. J., Warwicker, J., and Houslay, M. D. (2002) TAPAS-1, a novel microdomain within the unique N-terminal region of the PDE4A1 cAMP-specific phosphodiesterase that allows rapid, Ca^{2+} -triggered membrane association with selectivity for interaction with phosphatidic acid, *J. Biol. Chem.* 277, 28298–28309.
- Ghosh, S., Strum, J. C., Sciorra, V. A., Daniel, L., and Bell, R. M. (1996) Raf-1 kinase possesses distinct binding domains for phosphatidylserine and phosphatidic acid. Phosphatidic acid regulates the translocation of Raf-1 in 12-*O*-tetradecanoylphorbol-13-acetate-stimulated Madin-Darby canine kidney cells, *J. Biol. Chem.* 271, 8472–8480.
- Ghosh, S., and Bell, R. M. (1997) Regulation of Raf-1 kinase by interaction with the lipid second messenger, phosphatidic acid, *Biochem. Soc. Trans.* 25, 561–565.
- Bollen, M., and Stalmans, W. (1992) The structure, role, and regulation of type 1 protein phosphatases, *Crit. Rev. Biochem. Mol. Biol.* 27, 227–281.
- Cohen, P. T. (1997) Novel protein serine/threonine phosphatases: Variety is the spice of life, *Trends Biochem. Sci.* 22, 245–251.
- Chalfant, C. E., Ogretmen, B., Galadari, S. H., Kroesen, B. B., Pettus, B. J., and Hannun, Y. A. (2001) FAS activation induces dephosphorylation of SR proteins. Dependence on the de novo generation of ceramide and activation of protein phosphatase-1, *J. Biol. Chem.* 276, 13.
- Hubbard, M. J., and Cohen, P. (1993) On target with a new mechanism for the regulation of protein phosphorylation, *Trends Biochem. Sci.* 18, 172–177.
- Misteli, T., and Spector, D. L. (1996) Serine/threonine phosphatase 1 modulates the subnuclear distribution of pre-mRNA splicing factors, *Mol. Biol. Cell* 7, 1559–1572.
- Bollen, M. (2001) Combinatorial control of protein phosphatase-1, *Trends Biochem. Sci.* 26, 426–431.
- Wakula, P., Beullens, M., Ceulemans, H., Stalmans, W., and Bollen, M. (2003) Degeneracy and function of the ubiquitous RVXF motif that mediates binding to protein phosphatase-1, *J. Biol. Chem.* 278, 18817–18823.
- Jones, J. A., and Hannun, Y. A. (2002) Tight binding inhibition of protein phosphatase-1 by phosphatidic acid. Specificity of inhibition by the phospholipid, *J. Biol. Chem.* 277, 15530–15538.
- Rebecchi, M., Peterson, A., and McLaughlin, S. (1992) Phosphoinositide-specific phospholipase C- δ 1 binds with high affinity to phospholipid vesicles containing phosphatidylinositol 4,5-bisphosphate, *Biochemistry* 31, 12742–12747.
- Rost, B., Sander, C., and Schneider, R. (1994) PHD—An automatic mail server for protein secondary structure prediction, *Comput. Appl. Biosci.* 10, 53–60.
- Rost, B., and Sander, C. (1993) Improved prediction of protein secondary structure by use of sequence profiles and neural networks, *Proc. Natl. Acad. Sci. U.S.A.* 90, 7558–7562.

15. Rost, B. (1996) PHD: Predicting one-dimensional protein structure by profile-based neural networks, *Methods Enzymol.* 266, 525–539.
16. Maynes, J. T., Bateman, K. S., Cherney, M. M., Das, A. K., Luu, H. A., Holmes, C. F., and James, M. N. (2001) Crystal structure of the tumor-promoter okadaic acid bound to protein phosphatase-1, *J. Biol. Chem.* 276, 44078–44082.
17. Ito, M., Feng, J., Tsujino, S., Inagaki, N., Inagaki, M., Tanaka, J., Ichikawa, K., Hartshorne, D. J., and Nakano, T. (1997) Interaction of smooth muscle myosin phosphatase with phospholipids, *Biochemistry* 36, 7607–7614.
18. van Rossum, D. B., Patterson, R. L., Sharma, S., Barrow, R. K., Kornberg, M., Gill, D. L., and Snyder, S. H. (2005) Phospholipase C γ 1 controls surface expression of TRPC3 through an intermolecular PH domain, *Nature* 434, 99–104.

BI0505159